

The helion charge radius from laser spectroscopy of muonic helium-3 ions

Karsten Schuhmann,¹ Luis M. P. Fernandes,² François Nez,³ Marwan Abdou Ahmed,⁴ Fernando D. Amaro,² Pedro Amaro,⁵ François Biraben,³ Tzu-Ling Chen,⁶ Daniel S. Covita,⁷ Andreas J. Dax,⁸ Marc Diepold,⁹ Beatrice Franke,⁹ Sandrine Galtier,³ Andrea L. Gouvea,² Johannes Götzfried,⁹ Thomas Graf,⁴ Theodor W. Hänsch,⁹ Malte Hildebrandt,⁸ Paul Indelicato,³ Lucile Julien,³ Klaus Kirch,^{1,8} Andreas Knecht,⁸ Franz Kottmann,^{1,8} Julian J. Krauth,^{9,10} Yi-Wei Liu,⁶ Jorge Machado,⁵ Cristina M. B. Monteiro,² Françoise Mulhauser,⁹ Boris Naar,¹ Tobias Nebel,⁹ Joaquim M. F. dos Santos,² José Paulo Santos,⁵ Csilla I. Szabo,³ David Taqqu,^{1,8} João F. C. A. Veloso,⁷ Andreas Voss,⁴ Birgit Weichelt,⁴ Aldo Antognini,^{1,8,*} and Randolf Pohl^{9,10,†}

(The CREMA Collaboration)

¹*Institute for Particle Physics and Astrophysics, ETH Zurich, 8093 Zurich, Switzerland*

²*LIBPhys, Physics Department, Universidade de Coimbra, P-3004-516 Coimbra, Portugal*

³*Laboratoire Kastler Brossel, UPMC-Sorbonne Universités, CNRS, ENS-PSL Research University, Collège de France, 4 place Jussieu, case 74, 75005 Paris, France*

⁴*Institut für Strahlwerkzeuge, Universität Stuttgart, 70569 Stuttgart, Germany*

⁵*Laboratório de Instrumentação, Engenharia Biomédica e Física da Radiação (LIBPhys-UNL) e Departamento de Física da Faculdade de Ciências e Tecnologia da Universidade Nova de Lisboa, Monte da Caparica, 2892-516 Caparica, Portugal*

⁶*Physics Department, National Tsing Hua University, Hsincho 300, Taiwan*

⁷*i3N, Universidade de Aveiro, Campus de Santiago, 3810-193 Aveiro, Portugal*

⁸*Paul Scherrer Institute, 5232 Villigen, Switzerland*

⁹*Max-Planck-Institut für Quantenoptik, 85748 Garching, Germany*

¹⁰*Johannes Gutenberg Universität Mainz, Institut für Physik, QUANTUM, & Exzellenzcluster PRISMA⁺, 55099 Mainz, Germany*

(Dated: June 27, 2023)

Hydrogen-like light muonic ions, in which one negative muon replaces all the electrons, are extremely sensitive probes of nuclear structure, because the large muon mass increases tremendously the wave function overlap with the nucleus. Using pulsed laser spectroscopy we have measured three 2S-2P transitions in the muonic helium-3 ion ($\mu^3\text{He}^+$), an ion formed by a negative muon and bare helium-3 nucleus. This allowed us to extract the Lamb shift $E(2P_{1/2} - 2S_{1/2}) = 1258.598(48)^{\text{exp}}(3)^{\text{theo}}$ meV, the 2P fine structure splitting $E_{\text{FS}}^{\text{exp}} = 144.958(114)$ meV, and the 2S-hyperfine splitting (HFS) $E_{\text{HFS}}^{\text{exp}} = -166.495(104)^{\text{exp}}(3)^{\text{theo}}$ meV in $\mu^3\text{He}^+$. Comparing these measurements to theory we determine the rms charge radius of the helion (^3He nucleus) to be $r_h = 1.97007(94)$ fm. This radius represents a benchmark for few nucleon theories and opens the way for precision tests in ^3He atoms and ^3He -ions. This radius is in good agreement with the value from elastic electron scattering, but a factor 15 more accurate. Combining our Lamb shift measurement with our earlier one in $\mu^4\text{He}^+$ we obtain $r_h^2 - r_\alpha^2 = 1.0636(6)^{\text{exp}}(30)^{\text{theo}}$ fm² to be compared to results from the isotope shift measurements in regular He atoms, which are however affected by long-standing tensions. By comparing $E_{\text{HFS}}^{\text{exp}}$ with theory we also obtain the two-photon-exchange contribution (including higher orders) which is another important benchmark for ab-initio few-nucleon theories aiming at understanding the magnetic and current structure of light nuclei.

Keywords: muonic atoms, Lamb shift, laser spectroscopy, helion, nuclear charge radius

INTRODUCTION

Precise and accurate values of nuclear radii are necessary for advancing the theory prediction in simple atomic and molecular systems, that could be exploited to test bound-state Quantum Electro Dynamics (QED) predictions, to determine fundamental constants such as the Rydberg constant and the electron mass and to search for new physics [1]. Moreover these radii represent rigorous benchmarks for nuclear structure theory with the peculiar enhanced sensitivity to the long range behaviour of the nuclear wave functions. Spectacular advances have been obtained recently for nucleon-nucleon currents and form factors of light nuclei using nuclear interactions derived from chiral effective field theory which can be sys-

tematically improved [2–4]. On the experimental side, laser spectroscopy of muonic atoms with their exquisite sensitivity to nuclear properties has been recently established [5–7]. Owing to the 200 times larger muon mass compared to the electron mass, these muonic atoms (ions) where a single negative muon is orbiting a bare nucleus, have a dramatically enhanced sensitivity to the nuclear charge radii compared to regular atoms. This sensitivity arises from the enhanced overlap of the atomic wavefunction with the nucleus which scales with the third power of the orbiting particle mass (reduced mass). Indeed the leading-order finite-nuclear-size effect takes the form

$$\Delta E_{\text{FNS}}(n, l) = \frac{2}{3n^3} (Z\alpha)^4 m_r^3 r^2 \delta_{l0}, \quad (1)$$

where n is the principal quantum number, l the angular momentum, α the fine structure constant, Z the atomic number, m_r the reduced mass, and r the nuclear charge radius. The Kronecker δ_{l0} indicates that only S-states energy levels are affected in leading approximation by the finite size due to their overlap with the nucleus.

In this work, we present the measurement of three $2S \rightarrow 2P$ transitions of the muonic helium-3 ion $\mu^3\text{He}^+$ (a two-body ion formed by a negative muon and a bare ^3He nucleus) as shown in Fig. 1 from which we extracted the $2S$ - $2P$ Lamb shift, the $2S$ hyperfine splitting and the $2P$ fine splitting. From the Lamb shift we have then extracted the rms charge radius of the helion r_h with an unprecedented relative precision of 7×10^{-4} , improving the previous best value [8] from elastic electron scattering by a factor of 15. From the comparison between $2S$ -HFS and theory, we extracted the two-photon-exchange contribution which is the leading-order nuclear structure dependent contribution for the HFS. Hence, these measurements provide important benchmarks for nuclear theories, and pave the way for advancing precision tests of two- and three-body QED when combined with ongoing efforts in regular He atoms [9–16] and He^+ ions [17, 18].

The $2S$ - $2P$ transition frequencies were measured by pulsed laser spectroscopy at wavelengths around 850-940 nm (frequencies of 310-350 THz) to an accuracy of about 20 GHz corresponding to relative accuracies of about 50 ppm. The resonances were exposed by detecting the K_α X-ray of 8 keV energy emitted from $2P \rightarrow 1S$ de-excitation following a successful laser transition from the $2S$ to the $2P$ state. The 50 ppm measurement precision has to be compared to the energy shift caused by the finite-size effect (see Eq. (1)) that contributes as much as 25% to the $2S$ - $2P$ energy splitting owing to its $m_r^3 Z^4$ dependence. The binding energy of this hydrogen-like system, scaling as $Z^2 m_r$, is strongly enhanced compared to hydrogen, while the atomic size (Bohr radius) scaling as $1/Z m_r$ is strongly reduced making this atom immune to external perturbation. Because of its $m_r Z^4$ dependence, the decay rate from the $2P$ state is also vastly increased resulting in a $2P$ -linewidth of 319 GHz. This broad linewidth represents by far the main limitation to our experimental precision. Having in mind these energy scales, sensitivity to nuclear properties and immunity to external perturbations helps framing the requirements for the spectroscopy experiment and understanding of the experimental setup.

PRINCIPLE AND EXPERIMENTAL SETUP

$\mu^3\text{He}^+$ ions are formed in highly excited states by stopping a keV-energy muon in a low-pressure (2 mbar) ^3He gas target at room temperature and placed in a 5 T solenoid. The newly formed $\mu^3\text{He}^+$ ions deexcite to the $1S$ state in a fast (ns-scale) and complex cascade process

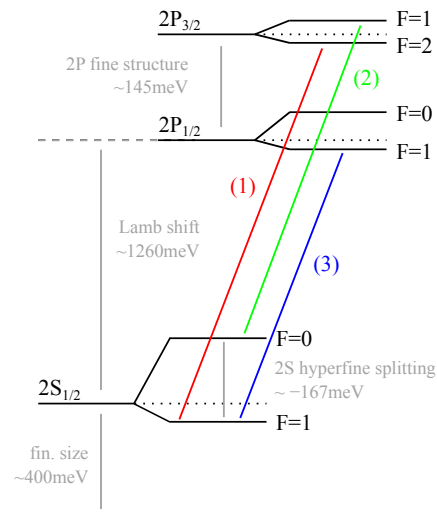


FIG. 1. Scheme (not to scale) of the $n = 2$ energy levels in $\mu^3\text{He}^+$ and the measured transitions. Due to the negative magnetic moment of the helion, the ordering of the hyperfine levels is reversed.

with a fraction of about 1% reaching the metastable $2S$ state whose lifetime is approximately $1.7 \mu\text{s}$ at this target pressure. This lifetime is sufficiently long to enable pulsed laser spectroscopy of the $2S$ - $2P$ splitting. For this purpose the muon entering the target is being detected to trigger a laser system that delivers a pulse to excite the $2S$ into the $2P$ state after a delay of about $1 \mu\text{s}$. The laser pulse is injected into a multipass cell formed by two elongated mirrors that fold the light back and forth to illuminate the elongated muon stopping volume. A successful laser excitation is established by detecting the 8 keV energy K_α X-ray from the $2P$ de-excitation into the ground state. This is accomplished using two rows of large area avalanche photodiodes (LAAPDs) placed above and below the muon stopping volume, respectively and covering 30% solid angle. The $2S$ - $2P$ resonances are eventually obtained by plotting the number of K_α X-rays detected in time coincidence with the laser light as a function of the laser frequency.

A sketch of the setup is shown in Fig. 2. The experiment has been performed at the $\pi\text{E}5$ beamline of the CHRISP facility at the Paul Scherrer Institute (PSI), Switzerland. Here, $102 \text{ MeV}/c$ negative pions are injected tangentially into a cyclotron trap (CT) formed by two coils generating a B-field with a magnetic-bottle geometry [19]. A fraction of the muons from the pion decays are trapped in the B-field of the CT. Passing multiple times a thin foil placed in the trap mid-plane, these muons are decelerated down to 20-40 keV energy. At this low energy, the electric field which is applied along the trap axis imparts sufficient longitudinal momentum to the muons so that they can escape the magnetic confinement of the CT in axial direction. The escaping muons

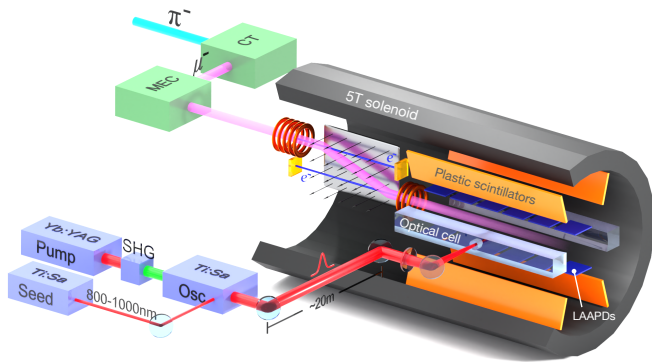


FIG. 2. Sketch of the experimental setup. CT cyclotron trap, MEC muon extraction channel, Ti:Sa Titanium-sapphire laser, Yb:YAG thin-disk laser, SHG second harmonic generation. The arrows indicate the electric field of the $E \times B$ Wien-filter.

are coupled into a toroidal magnetic field, the muon extraction channel (MEC), that acts as a momentum filter. The MEC transports the muons into a region of lower background where the spectroscopy experiment can be performed shielded from the large background of neutrons, gammas and other charged particles present in the CT. From the MEC toroidal field of 0.1 T, the muon beam is focused into the 5 T solenoid. Before entering the He target with an average rate of about 500s^{-1} , the muons are passing two stacks of few $\mu\text{g}/\text{cm}^2$ thin carbon foils placed at high voltages that serve two purposes: firstly they reduce the muon energy to few keV while obtaining some frictional cooling [20], and secondly they generate a muon entrance signal to trigger the laser system. The muon entrance signal is obtained by detecting the secondary electrons ejected from the carbon foils by the passing muon. The foils are biased to accelerate the electrons towards two plastic scintillators coupled to photomultipliers. An $E \times B$ Wien filter separates the muon from the electrons generated in the first stack of foils. To increase the laser trigger quality, i.e., to fire the laser only for muons which have maximal probability to stop in the He gas target, a fine selection of the muon momentum is performed. This is achieved requiring a coincidence with the optimal time-of-flight between the two electron signals from the two carbon stacks. The muons then pass a thin ($2\ \mu\text{g}/\text{cm}^2$) entrance window of Formvar before slowing down in the low-density He gas giving rise to a 20 cm long stopping distribution. The gas in the target is kept clean by a circulation system with a cold trap.

The detection of a randomly arriving muon triggers the pulsed laser system. With a delay of about $1\ \mu\text{s}$ the laser pulses of 5 mJ energy and 70 ns pulse length are coupled through a 0.6 mm diameter hole into a multi-pass cell formed by two elongated laser mirrors [21] which are shaped to match the muon stopping distribution. The laser system consists of a thin-disk Yb:YAG

oscillator-amplifier system [22, 23], a frequency doubling stage (SHG), and a Ti:Sapphire oscillator. The Ti:Sapphire oscillator is injection seeded by a Ti:Sapphire single-frequency cw laser which is stabilized to a calibrated Fabry-Perot and referenced to a wavemeter with a 60 MHz absolute accuracy. The wavemeter was calibrated using transition lines in ^{133}Cs and ^{83}Kr . From the laser laboratory the pulses are sent to the target region over a distance of $\sim 20\text{m}$. An active pointing stabilization ensures a stable coupling of the laser pulse into the optical cell. A $\lambda/2$ retardation plate combined with a polarizer is used to adjust from time to time the pulse energy and maintain it roughly at 5 mJ compensating for possible drifts. The time and spatial distribution of the laser light in the cell is monitored using several photodiodes embedded into the mirror substrates which detect the small amount of light leaking through the mirror coatings.

A waveform analysis was applied to the LAAPDs signals to improve energy and time resolutions and to disentangle electrons from X-ray events yielding a FWHM energy resolution of 16% at 8.2 keV [24]. As the experiment is taking place with only one muon at a time in the setup, the detection of the muon-decay electron after the detection of a 8 keV X-ray is used to sharpen the event selection: a reduction of the background by more than an order of magnitude was observed when implementing this muon-decay electron cut. To increase the detection efficiency for these MeV electrons which are curling in the magnetic field, four plastic scintillators were placed radially around the He target as shown in Fig. 2.

MEASUREMENT AND DATA ANALYSIS

The events used to expose the three 2S-2P resonances shown in Fig. 1 had to fulfill the following sequence: a muon is detected in the entrance counter, a K_α X-ray is detected in the LAAPDs in time coincidence with the laser light in the cavity, and a decay electron is detected afterwards in the electron counters (or LAAPDs). To obtain the resonances shown in Fig. 3, the number of these events is plotted versus the laser frequency and normalized to the number of prompt K_α X-rays so that variations of the number of muons and X-ray detection efficiency do not affect the results. The laser frequency was alternated on the two sides of the resonance every 1-2 hours to reduce a possible distortion of the measured resonance due to variations of the performance of the experimental setup. The injected pulse energy was limited to 5 mJ to avoid significant saturation effects and optically-induced damage of the cavity coating. Because a minimum pulse-to-pulse separation of about 2 ms was imposed on the laser system for increased stability, about half of the entering muons do not trigger the laser system. Yet these "laser-off events" are used to precisely mea-

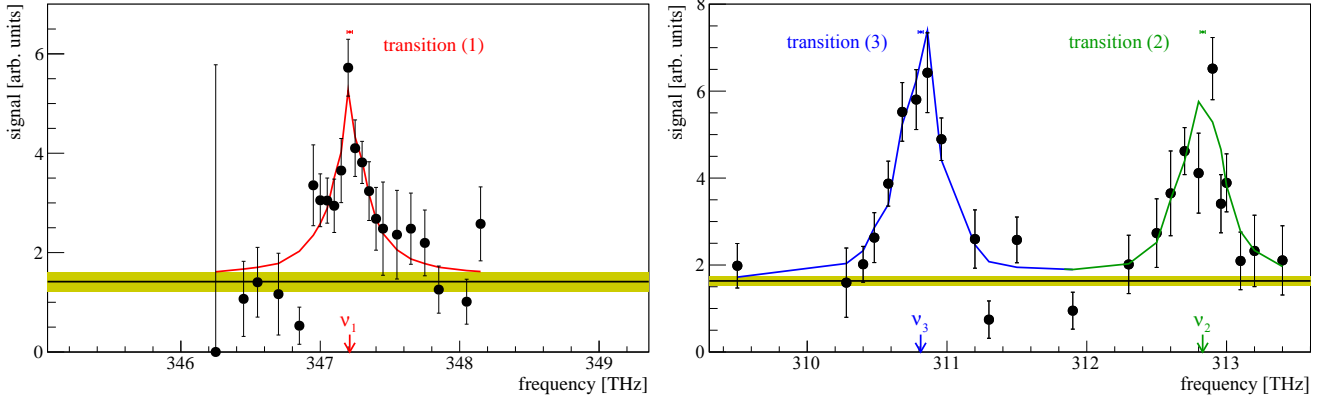


FIG. 3. Measured $2S \rightarrow 2P$ transitions in $\mu^3\text{He}^+$. The black data points show the number of laser-induced K_α X-ray events normalized to prompt K_α events. The data are fitted with a line shape model detailed in the main text. This model applies only at the measured points, and the colored lines only connect the fit points. The fitted center frequencies including their uncertainties are indicated by the colored points with error bar above the resonances. The yellow bands indicate the average $\pm 1\sigma$ backgrounds obtained from events where the laser was not fired.

sure the average background yielding the yellow bands in Fig. 3.

The transition (1) took about two weeks of continuous measurement, the transitions (2) and (3) have been measured at once, within about three weeks of continuous data taking. For the first transition, on resonance we observed a rate of 7-8 events/h including a background rate of ~ 1.5 events/h.

The center frequency of the measured lines is obtained by fitting the data with a line shape model. The model is a Lorentzian corrected for saturation effects and variations of the laser pulse energy measured for every shot. It can therefore only be evaluated at the position of each data point. This leads to the distortion in the line shape seen in Fig. 3. From the line shape fit we obtain following transition frequencies:

$$\nu_{\text{exp}}^{(1)} \equiv \nu(2P_{3/2}^{F=2} - 2S_{1/2}^{F=1}) = 347.212(20)^{\text{stat}}(1)^{\text{sys}} \text{ THz} \quad (2)$$

$$\nu_{\text{exp}}^{(2)} \equiv \nu(2P_{3/2}^{F=1} - 2S_{1/2}^{F=0}) = 312.830(21)^{\text{stat}}(1)^{\text{sys}} \text{ THz} \quad (3)$$

$$\nu_{\text{exp}}^{(3)} \equiv \nu(2P_{1/2}^{F=1} - 2S_{1/2}^{F=1}) = 310.814(20)^{\text{stat}}(1)^{\text{sys}} \text{ THz}. \quad (4)$$

The fit was done with a fixed linewidth of $\Gamma = 318.7$ GHz at FWHM. A separate fit with a free width resulted in widths that agreed with the theoretical one. Simply fitting Lorentzians yields line centers in agreement with the ones from the line shape model. The measured transition frequencies yield the energy splittings

$$\Delta E_{\text{exp}}^{(1)} = 1435.951(81) \text{ meV} \quad (5)$$

$$\Delta E_{\text{exp}}^{(2)} = 1293.759(86) \text{ meV} \quad (6)$$

$$\Delta E_{\text{exp}}^{(3)} = 1285.425(81) \text{ meV} \quad (7)$$

via the relation $1 \text{ meV} \hat{=} 241.798935 \text{ GHz}$.

The uncertainty of about 20 GHz, corresponding to about $6 \times 10^{-2} \Gamma$, is dominated by far by statistics. The largest systematic uncertainty stems from an upper limit to quantum interference effects [25] ($< 5 \times 10^{-4} \Gamma = 0.16 \text{ GHz}$) [26]. The uncertainty on the laser frequency is dominated by the chirp and the calibration of the wavemeter and conservatively given by 0.1 GHz. We corrected for the Zeeman shift caused by the 5T field by maximally 0.3 GHz (depending on the transition) so that the uncertainty of this correction is negligibly small in our context. Other systematic uncertainties (light shift, collisional effects, Stark shift etc.) are negligible compared with the precision of the measurement due to the strong binding, the small atomic size and the large separation between energy levels.

EXPERIMENTAL RESULTS

From the three transition measurements between 2S and 2P states with different fine and hyperfine sub-levels, it is possible to determine three quantities: we choose the Lamb shift $E_{\text{LS}} = \Delta E(2P_{1/2} - 2S_{1/2})$, the 2S hyperfine splitting E_{HFS} , and the 2P fine splitting $E_{\text{FS}} = \Delta E(2P_{3/2} - 2P_{1/2})$. The relations between the measured transition energies and these quantities are given by (see also Methods):

$$\Delta E_{\text{exp}}^{(1)} = E_{\text{LS}} - \frac{1}{4}E_{\text{HFS}} + E_{\text{FS}} - 9.23945(26) \text{ meV} \quad (8)$$

$$\Delta E_{\text{exp}}^{(2)} = E_{\text{LS}} + \frac{3}{4}E_{\text{HFS}} + E_{\text{FS}} + 15.05305(44) \text{ meV} \quad (9)$$

$$\Delta E_{\text{exp}}^{(3)} = E_{\text{LS}} - \frac{1}{4}E_{\text{HFS}} - 14.80851(18) \text{ meV} \quad (10)$$

where $E_{\text{HFS}} < 0$ and the numerical values of the last terms in Eqs. (8-10) arise from the 2P fine and hyperfine splittings, and include the contribution due to the mixing of the F=1 levels. These contributions can be calculated with great precision, because the 2P wave function of the hydrogen-like muonic He ion has negligible overlap with the nucleus, resulting in negligible contributions from nuclear size and structure corrections.

Note that the two most recent theory papers by Karshenboim et al., [27] and Pachucki et al. [28] use different conventions for the definition of the $2P_{1/2}$ and $2P_{3/2}$ centroids, which results in differing definitions of the Lamb shift. To obtain the constant terms in Eqs. (8-10) we have used the 2P levels calculated by Karshenboim et al., and modified them to account for the different definitions, such that our final result for the Lamb shift follows the convention of Pachucki et al. (see Methods).

We can solve the system of equations to obtain the experimental values of the Lamb shift, the 2S HFS and the 2P fine splitting:

$$E_{\text{LS}}^{\text{exp}} = 1258.612(86) \text{ meV} \quad (11)$$

$$E_{\text{HFS}}^{\text{exp}} = -166.485(118) \text{ meV} \quad (12)$$

$$E_{\text{FS}}^{\text{exp}} = 144.958(114) \text{ meV}. \quad (13)$$

The experimental value of the fine splitting $E_{\text{FS}}^{\text{exp}}$ is in excellent agreement with predictions $E_{\text{FS}}^{\text{th}} = 144.979(5) \text{ meV}$ [27], demonstrating consistency between our three muonic transitions measurements on the one hand, and the correctness of the theory of the 2P levels on the other. Owing to its much smaller uncertainty and consistency with measurements, we can use the theory value of the fine splitting to solve the system of equations Eqs. (8)-(10) to obtain improved values of the Lamb shift and 2S-HFS:

$$E_{\text{LS}}^{\text{exp}} = 1258.598(48)^{\text{exp}}(3)^{\text{theo}} \text{ meV} \quad (14)$$

$$E_{\text{HFS}}^{\text{exp}} = -166.496(104)^{\text{exp}}(3)^{\text{theo}} \text{ meV}. \quad (15)$$

The theoretical uncertainties are from the $\pm 0.005 \text{ meV}$ estimated higher-order corrections to the fine structure in Ref. [27].

THE HELION CHARGE RADIUS AND THE ISOTOPIC SHIFT

The theory prediction of the Lamb shift has been recently updated accounting for the contributions of various groups. It reads [28]

$$E_{\text{LS}}^{\text{th}}(r_h^2) = 1644.348(8) \text{ meV} - 103.383 r_h^2 \text{ meV/fm}^2 + 15.499(378) \text{ meV} \quad (16)$$

where the first term accounts for all QED corrections independent of the nuclear structure, the term proportional

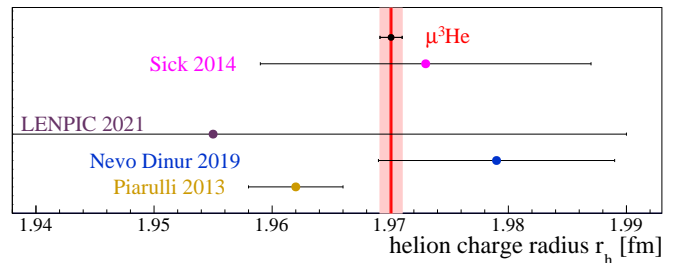


FIG. 4. Recent determinations of the ${}^3\text{He}$ nucleus (helion) charge radius. The dark and light bands indicate the experimental and total uncertainty in our measurement. The value of Sick of 1.973(14) fm [8] is from the world data on elastic electron scattering. The other values are recent predictions from nuclear few-body theory: Piarulli 1.962(4) fm [4, 31], Nevo Dinur 1.979(10) fm [32], and LENPIC collaboration 1.955(34) fm [33, 34]^a

^a We obtained this value using the point-proton structure radius and procedure explained in Ref. [33].

to r_h^2 accounts for the finite-size correction including radiative corrections to it, and the last term is a sum of all higher-order nuclear structure dependent contributions [2, 29, 30] which are dominated by the nuclear two- and three-photon exchange contributions (2PE and 3PE, respectively). Comparing this theory prediction with the measured Lamb shift $E_{\text{LS}}^{\text{exp}}$ we obtain the rms charge radius of the helion

$$r_h = 1.97007(12)^{\text{exp}}(93)^{\text{theo}} \text{ fm} = 1.97007(94) \text{ fm}. \quad (17)$$

This value is 15 times more precise than the previous best value from elastic electron- ${}^3\text{He}$ scattering of 1.973(14) fm [8], and in perfect agreement with it (see Fig. 4).

Our value could be further improved by almost an order of magnitude by advancing the predictions for the two-photon-exchange and three-photon-exchange contributions both for the nucleus and the nucleons [1, 2, 28].

It is interesting to compare this value with the helion charge radius as obtained from most recent nuclear theories which uses chiral effective field theory to describe the nuclear interaction and ab-initio methods to solve the quantum-mechanical few-body problem. Figure. 4 shows some of the most recent results taken from Ref. [4, 31, 33–35] depicting an overall satisfactory agreement between the measured value and the various predictions, and highlighting the role of the helion charge radius as benchmark for precision nuclear theory.

Spectroscopy of "normal" helium atoms can not yet provide precise values of the helion and alpha-particle charge radii, given the present uncertainty of the three-body atomic theory. Yet, in the isotopic shift, several cancellations take place in the theory [36] of the energy levels, so that values of $r_h^2 - r_\alpha^2$ [9–14] can be obtained where r_α is the alpha particle (${}^4\text{He}$) charge radius. The scattering of the values obtained so far shown in Fig. 5

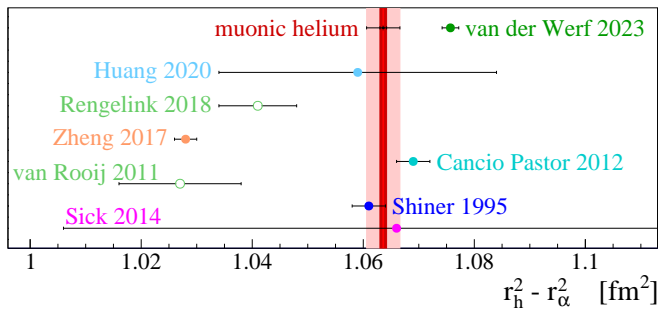


FIG. 5. Squared charge radius difference $r_h^2 - r_\alpha^2$ from measurements of the isotope shift in ordinary He atoms [9–16], compared to our value from muonic ions. The dark and light bands indicate the experimental and total uncertainty of our determination. The values of Shiner [9] and Cancio Pastor [11] have been corrected for improved theory calculations [36], but may lack a systematic correction due to quantum interference effects [25], as suggested in Ref. [37]. The value of Zheng [13] may have to be corrected for a systematic Doppler shift [38]. The most recent work from Amsterdam by van der Werf [16] supersedes the results from van Rooij [10] and Rengelink [14] by the same group.

however reveals some tensions that highlight the challenges faced by both theory and experiments.

It is thus interesting to address this quantity by considering the isotopic shift in muonic helium ions and presenting it in the form: [28]

$$r_h^2 - r_\alpha^2 = -\frac{E_{\text{LS}}^{\text{exp}}(\mu^3\text{He}^+)}{103.383 \frac{\text{meV}}{\text{fm}^2}} + \frac{E_{\text{LS}}^{\text{exp}}(\mu^4\text{He}^+)}{106.209 \frac{\text{meV}}{\text{fm}^2}} + 0.2585(30) \text{ fm}^2 \quad (18)$$

to take advantage of some cancellations in the nuclear structure contributions. Inserting the measured Lamb shift in $\mu^4\text{He}^+$ of $E_{\text{LS}}^{\text{exp}}(\mu^4\text{He}^+) = 1378.521(48) \text{ meV}$ [7] and $E_{\text{LS}}^{\text{exp}}(\mu^3\text{He}^+)$ from Eq. (11) into this expression [28, 39] we obtain

$$r_h^2 - r_\alpha^2 = 1.0636(6)^{\text{exp}}(30)^{\text{theo}} \text{ fm}^2. \quad (19)$$

This value can be compared with various isotopic shift measurements obtained in regular He atoms with two electrons [9–15], where long-standing discrepancies exist, see Fig. 5. Several novel systematic shifts were recently identified in these measurements [16, 37, 38], but nevertheless our result deviates by 3.6σ from the most recent and most precise value by the Amsterdam group [16]. Our measurements in muonic helium ions do not require the exquisite experimental accuracy of 10^{-12} reached in normal helium atoms, and are not sensitive to systematic effects. On the other hand, our results are limited by the nuclear structure effects which are much larger in muonic systems [2, 35, 40–43]. Clearly, more work is required to understand this 3.6σ deviation.

For completeness we quote here the updated Lamb

shift theory in $\mu^4\text{He}^+$ from Ref. [28]

$$E_{\text{LS}}^{\text{th}}(r_\alpha^2) = 1668.491(7) \text{ meV} - 106.209 r_\alpha^2 \text{ meV/fm}^2 + 9.276(433) \text{ meV}. \quad (20)$$

Combined with the Lamb shift in $\mu^4\text{He}^+$ we have measured in Ref. [7] this yields an updated ^4He (alpha particle) charge radius of $r_\alpha = 1.6786(12) \text{ fm}$ with a 45% larger uncertainty compared to our previous determination which used the theory summarized in [39]. The new r_α is obtained using the two-photon-exchange (TPE) contribution calculated solely from ab-initio theory [2] while previously we split it into a third-Zemach moment (Friar radius) contribution obtained from electron elastic scattering and a polarizability contribution from few-nucleon theories [2]. Because this splitting could lead to some inconsistencies [28], we now opt for the solution fully based on few-body theories [2].

NUCLEAR-STRUCTURE CONTRIBUTION FOR THE 2S HFS

By comparing the measured 2S-HFS $E_{\text{HFS}}^{\text{exp}}$ in $\mu^3\text{He}^+$ with the corresponding theory prediction [44]

$$E_{\text{HFS}}^{\text{th}} = -172.7457(89) \text{ meV} + E_{\text{HFS}}^{\text{nucl. struct.}} \quad (21)$$

we extract the nuclear structure-dependent contributions (2PE and higher orders) to the 2S hyperfine splitting

$$E_{\text{HFS}}^{\text{nucl. struct.}} = 6.25(10) \text{ meV}, \quad (22)$$

with an uncertainty arising basically only from the statistical uncertainties of the measurements. Subtracting the elastic part of the two-photon-exchange contribution $\Delta E_{2\text{PE}}^{\text{Zemach}} = 2.5836 \text{ meV/fm}$ $r_Z = 6.53(4) \text{ meV}$, where $r_Z = 2.528(16) \text{ fm}$ is the Zemach radius of the ^3He nucleus [8, 35] from $E_{\text{HFS}}^{\text{nucl. struct.}}$, we can obtain a value for the hitherto unknown polarizability contribution to the 2S hyperfine splitting of $-0.28(10) \text{ meV}$ (that includes also higher-order contributions). This represents an important benchmark to refine our understanding of the magnetic structure of the ^3He nucleus. It also allows, using appropriate scaling, to predict the nuclear structure contribution of the ground-state hyperfine splitting in $\mu^3\text{He}^+$ restricting considerably the range where this resonance has to be searched for.

CONCLUSION AND OUTLOOK

Laser spectroscopy of $\mu^3\text{He}^+$ and $\mu^4\text{He}^+$ [7] ions provides precision values of ^3He and ^4He charge radii and two-photon-exchange contributions, that serve as benchmarks [45–47] for few-body ab-initio nuclear theories [48],

driving the theory to new levels of precision. The nuclear theory [48] is challenged to scrutinize its approximations [31], to systematically improve the nuclear interaction [3, 45–47, 49, 50] and the formalism [2, 35, 40, 41] while finding novel methods to evaluate the uncertainties [42, 43].

The precise knowledge of r_h and r_α reduces the uncertainty of the nuclear-structure-dependent contributions in He and He⁺ [17]. This paves the way for bound-state QED tests for two-body (He⁺) and three-body (He) systems to an unprecedented level of accuracy [1, 51, 52]. The Lamb shift theory in He has undergone a spectacular advance in recent years, completing the calculation up to terms of order $\alpha^7 m$ [53]. Once the remaining discrepancies are solved there, electronic helium atoms and ions will provide more accurate charge radii [17, 18], because of the smaller higher-order nuclear structure effects in these electronic systems. Using Eqs. (16),(20), our measurements in muonic He ions will then yield the most precise experimental values for the nuclear structure contributions (beyond the leading finite-size effect). Finally, of course, comparison of results from electronic [16] and muonic systems can be used to search for physics beyond the Standard Model [1].

METHODS

To arrive at Eqs. (8-10) we used the most recent calculations for the 2P level structure by Karshenboim et al. [27], and of the 2S Lamb shift by Pachucki et al. [28].

However, these papers use a different convention for the definition of the $2P_{1/2}$ and $2P_{3/2}$ level centroids, and of the Lamb shift. These differences come from the treatment of the Barker-Glover (BG) and Brodsky-Parsons (BP) terms.

Both terms are not part of what Karshenboim et al. [27] denote as "Lamb shift", but it is named "Unperturbed quantum mechanics" therein, and their sum is -0.0032 meV (Tab. X No. 0), which is the sum of the "BP*" and "BG*" terms listed in Tab.II, therein.

The "BG*" term of 0.1265 meV in Ref. [27] is also already included in the Lamb shift in Pachucki et al. [28], term as " $(Z\alpha)^4$ recoil", term III.C, hence this term contributes equally to the $2P_{1/2}$ - $2S_{1/2}$ energy difference in both conventions.

The "BP*" term of -0.1298 meV, however, is not considered in Pachucki et al. [28], because it only arises because of the hyperfine level mixing of the F=1 levels.

Thus, to make the Lamb shift of Pachucki et al. [28] compatible with the definitions of the 2P levels in Karshenboim et al. [27], we define the position of our $2P_{1/2}$ centroid as

$$E(2P_{1/2}) = E(2S_{1/2}) + E_{LS} - 0.1298 \text{ meV}, \quad (23)$$

where 0.1298 meV is the "BP*" term in Ref. [27], Tab.II, No. 0.4. This ensures that our measured Lamb shift E_{LS} agrees with the convention of Pachucki, while the FS and 2P-HFS splittings follow the convention of Karshenboim, where the $2P_{1/2}$ and $2P_{3/2}$ levels are the weighted average of the physical hyperfine levels.

This gives for the transition energies we measured

$$\Delta E_{\text{exp}}^{(1)} = E_{LS} + E_{BP*} - \frac{1}{4}E_{\text{HFS}} + E_{\text{FS}} + \frac{3}{8}E_{\text{HFS}}^{(P3/2)} \quad (24)$$

$$\Delta E_{\text{exp}}^{(2)} = E_{LS} + E_{BP*} + \frac{3}{4}E_{\text{HFS}} + E_{\text{FS}} - \frac{5}{8}E_{\text{HFS}}^{(P3/2)} \quad (25)$$

$$\Delta E_{\text{exp}}^{(3)} = E_{LS} + E_{BP*} - \frac{1}{4}E_{\text{HFS}} + \frac{1}{4}E_{\text{HFS}}^{(P1/2)}, \quad (26)$$

where $E_{\text{HFS}}^{(P1/2)} = -58.7150(7)$ meV and $E_{\text{HFS}}^{(P3/2)} = -24.2925(7)$ meV are the 2P hyperfine level splittings [27] and $E_{BP*} = -3/4 * 0.17302(2)$ meV (see Tab. XIV in Ref. [27]) is the above-mentioned "BP*" term of -0.1298 meV [27].

ACKNOWLEDGMENTS

This paper is dedicated to Ingo Sick and Wim Vassen. We thank Sonia Bacca, Kjeld Eikema, Evgeny Epelbaum, Franziska Hagelstein, Savely Karshenboim, Simone Li Muli, Vadim Lensky, Laura Marcucci, Ulf Meißner, Krzysztof Pachucki, Leo Simons, and Kees Steinebach for fruitful discussions. We acknowledge support from the European Research Council (ERC) through StG. #279765, and CoG. #725039; from the Deutsche Forschungsgemeinschaft (DFG, German Research Foundation) under Germany's Excellence Strategy EXC PRISMA+ (390831469), European Union's Horizon 2020 research and innovation programme under grant agreement STRONG - 2020 - No 824093; from FEDER and FCT via project PTDC/FIS-NUC/0843/2012, from FCT Contract No. SFRH/BPD/76842/2011, and SFRH/BPD/92329/2013, SFRH/BD/52332/2013; from DFG-GR_3172/9-1, from SNF projects 2200021L_138175, 200020_159755, 200021_165854, 200020_197052 and by the ETH Femtosecond and Attosecond Science and Technology (ETH-FAST) initiatives as part of the NCCR MUST program.

* aldo.antognini@psi.ch

† pohl@uni-mainz.de

[1] A. Antognini, F. Hagelstein, and V. Pascalutsa. *Ann. Rev. Nucl. Part. Sci.* **72**, 389 (2022).

- [2] C. Ji, S. Bacca, N. Barnea, et al. *Journal of Physics G: Nuclear and Particle Physics* **45**, 093002 (2018).
- [3] E. Epelbaum. ‘Towards high-precision nuclear forces from chiral effective field theory’. In ‘6th International Conference Nuclear Theory in the Supercomputing Era’, (2019).
- [4] M. Piarulli, L. Girlanda, L. E. Marcucci, et al. *Phys. Rev. C* **87**, 014006 (2013).
- [5] A. Antognini, F. Nez, K. Schuhmann, et al. *Science* **339**, 417 (2013).
- [6] R. Pohl, F. Nez, L. M. P. Fernandes, et al. *Science* **353**, 669 (2016).
- [7] J. J. Krauth, K. Schuhmann, M. Abdou Ahmed, et al. *Nature* **589**, 527 (2021).
- [8] I. Sick. *Phys. Rev. C* **90**, 064002 (2014).
- [9] D. Shiner, R. Dixson, and V. Vedantham. *Phys. Rev. Lett.* **74**, 3553 (1995).
- [10] R. van Rooij, J. S. Borbely, J. Simonet, et al. *Science* **333**, 196 (2011).
- [11] P. Cancio Pastor, L. Consolino, G. Giusfredi, et al. *Phys. Rev. Lett.* **108**, 143001 (2012).
- [12] V. Patkóš, V. A. Yerokhin, and K. Pachucki. *Phys. Rev. A* **94**, 052508 (2016). [arXiv:1610.04060].
- [13] X. Zheng, Y. Sun, J.-J. Chen, et al. *Phys. Rev. Lett.* **119**, 263002 (2017).
- [14] R. J. Rengelink, Y. van der Werf, R. P. M. J. W. Notermans, et al. *Nat. Phys.* (2018). [arXiv:1804.06693].
- [15] Y.-J. Huang, Y.-C. Guan, J.-L. Peng, et al. *Phys. Rev. A* **101**, 062507 (2020).
- [16] Y. van der Werf, K. Steinebach, R. Jannin, et al. *arXiv 2306.02333* (2023).
- [17] J. Moreno, F. Schmid, J. Weitenberg, et al. *Eur. Phys. J. D* **77**, 67 (2023).
- [18] J. Krauth, L. Dreissen, C. Roth, et al. *PoS FFK2019*, 49 (2019).
- [19] D. Gotta and L. M. Simons. *SciPost Phys. Proc.* **5**, 013 (2021).
- [20] M. Mühlbauer, H. Daniel, F. Hartmann, et al. *Hyp. Interact.* **119**, 305 (1999).
- [21] J. Vogelsang, M. Diepold, A. Antognini, et al. *Opt. Express* **22**, 13050 (2014).
- [22] A. Antognini, K. Schuhmann, F. D. Amaro, et al. *IEEE J. Quant. Electr.* **45**, 993 (2009).
- [23] K. Schuhmann, M. A. Ahmed, A. Antognini, et al. *Proc. SPIE* **9342**, 93420U (2015).
- [24] M. Diepold, L. M. P. Fernandes, J. Machado, et al. *Rev. Sci. Instrum.* **86**, 053102 (2015).
- [25] R. C. Brown, S. Wu, J. V. Porto, et al. *Phys. Rev. A* **87**, 032504 (2013).
- [26] P. Amaro, B. Franke, J. J. Krauth, et al. *Phys. Rev. A* **92**, 022514 (2015).
- [27] S. G. Karshenboim, E. Y. Korzinin, V. A. Shelyuto, et al. *Phys. Rev. A* **96**, 022505 (2017).
- [28] K. Pachucki, V. Lensky, F. Hagelstein, et al. *arXiv* **2212.13782** (2022).
- [29] C. E. Carlson, M. Gorchtein, and M. Vanderhaeghen. *Phys. Rev. A* **95**, 012506 (2017).
- [30] K. Pachucki, V. Patkóš, and V. A. Yerokhin. *Phys. Rev. A* **97**, 062511 (2018).
- [31] L. E. Marcucci, F. Gross, M. T. Pena, et al. *J. Phys. G* **43**, 023002 (2016).
- [32] N. Nevo Dinur, O. J. Hernandez, S. Bacca, et al. *Physical Review C* **99** (2019).
- [33] P. Maris, E. Epelbaum, R. J. Furnstahl, et al. *Phys. Rev. C* **103**, 054001 (2021).
- [34] P. Maris et al. *Phys. Rev. C* **106**, 064002 (2022).
- [35] N. Nevo Dinur, O. J. Hernandez, S. Bacca, et al. *Phys. Rev. C* **99**, 034004 (2019).
- [36] K. Pachucki, V. c. v. Patkóš, and V. A. Yerokhin. *Phys. Rev. A* **95**, 062510 (2017).
- [37] A. Marsman, E. A. Hessels, and M. Horbatsch. *Phys. Rev. A* **89**, 043403 (2014).
- [38] J.-L. Wen, J.-D. Tang, J.-F. Dong, et al. *Phys. Rev. A* **107**, 042811 (2023).
- [39] M. Diepold, B. Franke, J. J. Krauth, et al. *Ann. Phys.* **396**, 220 (2018). [arXiv:1606.05231].
- [40] O. J. Hernandez, C. Ji, S. Bacca, et al. *Phys. Rev. C* **100**, 064315 (2019).
- [41] A. A. Filin, D. Möller, V. Baru, et al. *Phys. Rev. C* **103**, 024313 (2021).
- [42] B. Acharya, S. Bacca, F. Bonaiti, et al. *arXiv* **2210.04632** (2022).
- [43] S. S. L. Muli, B. Acharya, O. J. Hernandez, et al. *J. Phys. G* **49**, 105101 (2022).
- [44] B. Franke, J. J. Krauth, A. Antognini, et al. *Eur. Phys. J. D* **71**, 341 (2017). [arXiv:1705.00352].
- [45] A. Ekström, G. R. Jansen, K. A. Wendt, et al. *Phys. Rev. C* **91**, 051301 (2015).
- [46] J. E. Lynn, I. Tews, J. Carlson, et al. *Phys. Rev. C* **96**, 054007 (2017).
- [47] J. Vanasse. *Phys. Rev. C* **98**, 034003 (2018).
- [48] H.-W. Hammer, S. König, and U. van Kolck. *Rev. Mod. Phys.* **92**, 025004 (2020).
- [49] H. Krebs, E. Epelbaum, and U. G. Meißner. *Few Body Syst.* **60**, 31 (2019).
- [50] P. Reinert, H. Krebs, and E. Epelbaum. *Phys. Rev. Lett.* **126**, 092501 (2021).
- [51] S. G. Karshenboim, A. Ozawa, V. A. Shelyuto, et al. *Phys. Lett. B* **795**, 432 (2019).
- [52] V. A. Yerokhin, K. Pachucki, and V. Patkóš. *Ann. d. Phys. (Berlin)* **531**, 1800324 (2019).
- [53] V. Patkóš, V. A. Yerokhin, and K. Pachucki. *Phys. Rev. A* **103**, 042809 (2021).